Femtosecond light pulse propagation through metallic nanohole arrays: The role of the dielectric substrate

Roland Müller, Claus Ropers and Christoph Lienau

Max-Born-Institut für Nichtlineare Optik und Kurzzeitspektroskopie, Max-Born-Straße 2A, 12489 Berlin, Germany
rmueller@mbi-berlin.de

http://www.mbi-berlin.de

Abstract: We study theoretically ultrafast light propagation through a periodic array of holes in a silver film deposited on a dielectric substrate using a three-dimensional finite-difference time-domain (FDTD) simulation. We focus on studying the effects of the coherent coupling between resonant surface plasmon polariton (SPP) excitations at the top and bottom interfaces of the metal film on the transmission dynamics. In a free standing film, the SPP excitations at both interfaces are fully in resonance and pronounced temporal oscillations in the energy flow between the bottom and top interfaces give evidence for coupling between the $(\pm 1,0)$ SPP modes via photon tunneling through the holes. Variation of the dielectric constant of the substrate lifts the energetic degeneracy between the two modes and thus decreases the coupling and suppresses the energy oscillations. New SPP-enhanced transmission peaks appear when higher order modes at the substrate/metal interface are brought into resonance with the $(\pm 1,0)$ air/metal resonance and efficient mode coupling is achieved. Both temporal transmission dynamics and near-field mode profiles are reported and their implications for tailoring the optical properties of these two-dimensional plasmonic crystals are discussed.

OCIS codes: (050.0050) Diffraction and gratings, (240.6680) Surface plasmons, (310.6860) Thin films, optical properties, (320.2250) Femtosecond phenomena, (999.9999) Nano-optics

References and links

1. T. W. Ebbesen, H. J. Lezec, H. F. Ghaemi, T. Thio, and P. A. Wolff, "Extraordinary optical transmission through sub-wavelength hole arrays," Nature **391**, 667-669 (1998).
2. H. F. Ghaemi, T. Thio, D. E. Grupp, T. W. Ebbesen, and H. J. Lezec, "Surface plasmons enhance optical transmission through subwavelength holes," Phys. Rev. B **58**, 6779-6782 (1998).
3. S. C. Kitson, W. L. Barnes, and J. R. Sambles, "Full photonic band gap for surface modes in the visible," Phys. Rev. Lett. **77**, 2670-2673 (1996).
4. W. L. Barnes, T. W. Preist, S. C. Kitson, and J. R. Sambles, "Physical origin of photonic energy gaps in the propagation of surface plasmons on gratings," Phys. Rev. B **54**, 6227-6224 (1996).
5. U. Schröter and D. Heitmann, "Grating couplers for surface plasmons excited on thin metal films in the Kretschmann-Raether configuration, " Phys. Rev. B **60**, 4992-4999 (1999).
6. D. S. Kim, S. C. Hohng, V. Malyarchuk, Y. C. Yoon, Y. H. Ahn, K .J. Yee, J. W. Park, J. Kim, Q. H. Park, and C. Lienau, "Microscopic origin of surface-plasmon radiation in plasmonic band-gap nanostructures," Phys. Rev. Lett. **91**, 143901 (2003).
7. H. Raether, *Surface plasmons*, Springer Tracts in Modern Physics Vol. **111**, (Springer, Berlin, 1988).
8. U. Schröter and D. Heitmann, "Surface-plasmon-enhanced transmission through metallic gratings," Phys. Rev. B **58,** 15419-15421 (1998).
9. M. M. J. Treacy, "Dynamical diffraction in metallic optical gratings," Appl. Phys. Lett. **75**, 606-608 (1999).
10. J. A. Porto, F. J. Garcia–Vidal, and J. B. Pendry, "Transmission resonances on metallic gratings with very narrow slits," Phys. Rev. Lett. **83**, 2845-2848 (1999).

#4821 - $15.00 US Received 16 July 2004; revised 23 September 2004; accepted 2 October 2004

11. Q. Cao and P. Lalanne, "Negative role of surface plasmons in the transmission of metallic gratings with very narrow slits," Phys. Rev. Lett. **88**, 057403 (2002).
12. E. Popov, M. Neviere, S. Enoch, and R. Reinisch, "Theory of light transmission through subwavelength periodic hole arrays," Phys. Rev. B **62**, 16100-16108 (2000).
13. L. Salomon, F. Grillot, A. V. Zayats, and F. de Fornel, "Near-field distribution of optical transmission of periodic subwavelength holes in a metal film,". Phys. Rev. Lett. **86**, 1110-1113 (2001).
14. L. Martin – Moreno, F. J. Garcia-Vidal, H. J. Lezec, K. M. Pellerin, T. Thio, J. B. Pendry, and T. W. Ebbesen, "Theory of extraordinary optical transmission through subwavelength hole arrays," Phys. Rev. Lett. **86,** 1114-1117 (2001).
15. S. Enoch, E. Popov, M. Neviere, and R. Reinisch, "Enhanced light transmission by hole arrays," J. Opt. A: Pure Appl. Opt. **4**, S83-S87 (2002).
16. S. A. Darmanyan and A. V. Zayats, "Light tunneling via resonant surface plasmon polariton states and the enhanced transmission of periodically nanostructured metal films: An analytical study," Phys. Rev. B **67**, 035424 (2003).
17. F. I. Baida and D .Van Labeke, "Three-dimensional structures for enhanced transmission through a metallic film: Annular aperture arrays," Phys. Rev.B **67**, 155314 (2003).
18. A. V. Zayats and I. I. Smolyaninov, "Near-field photonics:surface plasmon polaritons and localized surface plasmons, " J.. Opt. A: Pure Appl. Opt. **5**, S16-S50 (2003).
19. P. N. Stavrinou and L. Solymar, "Pulse delay and propagation through subwavelength metallic slits," Phys. Rev. E **68**, 066604 (2003).
20. A. Dechant and A.Y.Elezzabi, "Femtosecond optical pulse propagation in subwavelength metallic slits," Appl. Phys. Lett. **84** , 4678-4680 (2004).
21. R. Müller, V. Malyarchuk, and C. Lienau, "A three-dimensional theory on light-induced near-field dynamics in a metal film with a periodic array of nanoholes," Phys. Rev. B **68**, 205415 (2003).
22. S. C. Hohng, Y. C. Yoon, D. S. Kim, V. Malyarchuk, R. Müller, Ch. Lienau, J. W. Park, K. H. Yoo, J. Kim, H. Y. Ryu, and Q. H. Park, "Light emission from the shadows: surface plasmon nano-optics at near and far fields," Appl. Phys. Lett. **81**, 3239-3241 (2002).
23. A. Krishnan, T. Thio, T. J. Kim, H. J. Lezec, T. W. Ebbesen, P. A. Wolff, J. Pendry, L. Martin-Moreno, and F. J. Garcia-Vidal, "Evanescently coupled resonance in surface plasmon enhanced transmission," Opt. Comm. **200**, 1-7 (2001).
24. A. Dogariu, T. Thio, L. J. Wang, T. W. Ebbesen, and H. J. Lezec, "Delay in light transmission through small apertures," Opt. Lett. **26**, 450-452 (2001).
25. H. Cao and A. Nahata, " Influence of aperture shape on the transmission properties of a periodic array of subwavelength apertures," Opt. Express **12,** 3664-3672 (2004).
26. P. B. Johnson and R. W. Christy, "Optical constants of noble metals," Phys. Rev. B **6**, 4370-4379 (1972).
27. E. D. Palik (Ed.), *Handbook of optical constants of solids* (Academic Press, San Diego,1985)
28. B. Lamprecht, J. R. Krenn, G. Schider, H. Ditlbacher, M. Salerno, N. Felidj, A. Leitner, and F. R. Aussenegg, "Surface plasmon propagation in microscale metal stripes," Appl. Phys. Lett. **79**, 51-53 (2001).
29. A. Taflove and S. C. Hagness, *Computational Electrodynamics. The Finite- Difference Time-Domain Method*, 2nd ed. (Artech House, Boston. 2000).
30. St. A. Cummer, "An analysis of new and existing FDTD methods for isotropic cold plasma and a method for improving their accuracy," IEEE Trans. Antennas Propag. **45**, 392-400 (1997).
31. R. E. Collin, *Field theory of guided waves* (Mc Graw-Hill, New York, 1960).
32. H. A. Bethe, "Theory of diffraction by small holes," Phys. Rev. **66**, 163-182 (1944).
33. C. J. Bouwkamp, "On Bethe's theory of diffraction by small holes," Philips Res. Rep. **5**. 321-332 (1950).
34. M. Sarrazin, J.-P. Vigneron, and J.-M. Vigoureux, "Role of Wood anomalies in optical properties of thin metallic films with a bidimensional array of subwavelength holes," Phys. Rev. B. **67**, 085415 (2003)
35. C. Genet, M. P. van Exter, and J. P. Woerdman, "Fano-type interpretation of red shifts and red tails in hole array transmission spectra," Opt. Commun. **225**, 331-336 (2003).

1. Introduction

Light propagation in periodically nanostructured metal films has been a subject of intense experimental and theoretical investigations in recent years. These studies gave evidence for the existence of unexpected transmission properties [1,2] and photonic energy band gaps [1-6]. Both effects have been connected with surface plasmon polaritons (SPPs), i.e., electromagnetic surface waves that propagate along the interface between a metal and a dielectric [7].

Ebbesen and coworkers first observed transmission spectra with extraordinarily high light transmission at certain wavelengths in metal films perforated with periodic arrays of

#4821 - $15.00 US Received 16 July 2004; revised 23 September 2004; accepted 2 October 2004

nanometer holes [1,2]. The transmission resonances are energetically close to SPP resonances at the corresponding metal/dielectric interfaces. It is believed that the excited SPP waves can support the energy transport through the holes and give rise to the enhanced transmission observed in the experiments.

Different aspects of light transmission through perforated metal films have been discussed in a variety of theoretical papers. Among them are time-independent simulations of light transmission through metallic films with one-dimensional slits [8-11], periodic arrays of nanometer-sized holes [12-16] and periodic annular aperture arrays [17]. For a recent review see Ref. [18]. Only few theoretical papers deal with SPP dynamics in perforated metal films: optical pulse propagation through one-dimensional slit arrays were studied to some extent in Ref. [19] and [20]. We have recently reported the first space- and time-resolved study of ultrafast light transmission through a metal film perforated with nanoholes [21].

Experimental near-field scanning optical microscopy (NSOM) studies of such nanohole arrays give direct evidence for SPP excitations and insight into the spatial SPP mode profiles [22]. In general, the SPP excitations at the two interfaces of such an array cannot be considered as independent entities but represent a pair of coupled modes. Their coupling depends on the dielectric constants of the sub- and superstrates, below and above the metal film. Transmission spectra for different dielectric constants were measured and theoretically modeled in [23]. Strongest coupling was found for identical dielectric constants of the sub- and superstrates. In this case, the SPP resonances at the two interfaces coincide and particularly large transmission enhancement is expected. A first experimental study of ultrafast light propagation through metallic nanohole arrays reports a 10 fs time delay [24]. Besides these experiments in the optical frequency range also the transmission of THz pulses was experimentally studied [25].

In a previous paper [21], we theoretically studied this coupling for a nanohole array in a free-standing silver film, with air as the dielectric medium at both interfaces. The coupled system was excited by a femtosecond light pulse, shorter in duration than the relevant damping and coupling times, and the subsequent light scattering dynamics was investigated in a FDTD simulation. We showed that the interaction between $(\pm 1,0)$ SPP resonances at the two interfaces of the silver film, gives rise to pronounced temporal oscillations in the field intensity transmitted through the nanoholes. Both the damping time and the period of these oscillations depend significantly on the hole diameter [6,21].

Here, we use the theoretical model of [21] and consider now an additional dielectric substrate on which the metal film is deposited. Ultrafast light transmission is studied with 10fs light pulses at $\lambda_{in} =$ 530 nm, close to the SPP resonance at the top air/metal interface for different values of the substrate refractive index $1 \le n_s < 2$. The aim of this paper is to investigate the effects of the coherent coupling between SPP excitations at the top and bottom interfaces on enhanced transmission through metallic nanohole arrays. Coupling between the $(\pm 1,0)$ air/metal SPP and different orders of substrate/metal SPP resonances is evidenced and its effect on enhanced transmission is discussed. The outline of the paper is as follows. In Section 2 we describe briefly our model. Section 3 presents simulations of the time-dependent energy flow through the nanohole channels and the energy densities inside the holes at the two interfaces for different values of n_s. In Section 4 we show spatial distributions of SPP near-field mode profiles on both interfaces at a fixed instant in time, after the incident pulse has vanished, and Section 5 presents movie sequences on time-dependent spatial SPP distributions. A summary and conclusions drawn from our calculations are given in Section 6.

2. Theoretical model

We study light propagation through a silver film of thickness h = 100 nm, perforated with a periodic hole array of period a_0 = 500 nm and hole diameter d = 125 nm. The film is deposited on a dielectric substrate and extends to infinity in the x and y direction. An x-polarized Gaussian pulse of 10-fs full width at half maximum (FWHM) is propagating in z-direction

#4821 - $15.00 US Received 16 July 2004; revised 23 September 2004; accepted 2 October 2004

and illuminates the metal at normal incidence, see Fig. 1.

Light propagation in the metal is described by Maxwell's equations that are coupled to an equation for the light-induced oscillations of quasi-free electrons in the metal (Drude model)

$$\vec{\nabla}\times\vec{E}=-\mu_0\frac{\partial\vec{H}}{\partial t} \tag{1a}$$

$$\vec{\nabla}\times\vec{H}=\varepsilon\varepsilon_0\frac{\partial\vec{E}}{\partial t}+\vec{J} \tag{1b}$$

$$\frac{\partial\vec{J}}{\partial t}+\gamma\vec{J}=\varepsilon_0\omega_p{}^2\vec{E}\,, \tag{1c}$$

where $\vec{E}$ and $\vec{H}$ are the electric and magnetic field vectors, respectively. $\vec{J}$ is a current density (A/cm^2) corresponding to the time derivative $\vec{J}=\partial\vec{P}/\partial t$ of the metal polarization. Outside the metal film $\vec{J}\equiv 0$. The parameter ε is the relative dielectric constant, with $\varepsilon=1$ for both air and metal and $\varepsilon=n_s^2$ for the substrate. $\varepsilon=1$ for the metal was chosen assuming that the optical properties of interest in the metal are described by quasi-free electrons in the conduction band, Eq. (1c), while the contribution of bound electrons in deeper bands is of minor importance. ω_p is the plasma frequency of the metal and γ a damping rate characterizing Ohmic absorption losses. Both parameters are related to the complex dielectric function of the metal ε_m by

$$\varepsilon_m(\omega)=1-\frac{\omega_p^2}{\omega^2+i\gamma\omega}\,. \tag{2}$$

corresponding to the dispersion relation following from Eqs (1a-c). Assuming $\varepsilon_m=-12.5+i0.4$ at $\omega_{in}=2\pi c/\lambda_{in}$ [26], one gets $\hbar\omega_p$ = 8.6 eV and $\hbar\gamma=75$ meV. These values of ε_m are somewhat different from those in Ref. [27], but in better agreement with measured SPP propagation lengths [28].

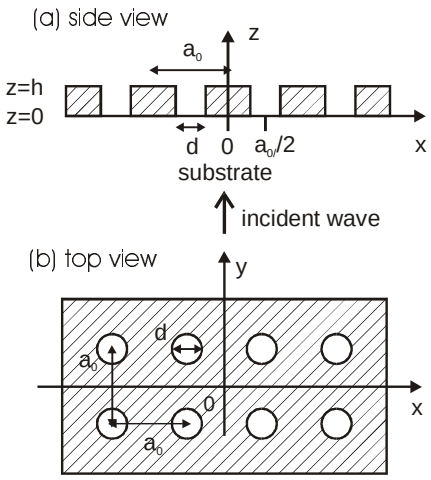

Fig. 1. Schematic of a metal film perforated with an array of holes and deposited on a substrate with a refractive index n_s. The medium above the film is air. a_0 is the lattice constant, *d* the hole diameter and *h* the film thickness. (a) Cross section through *x*-*z* plane. The input wave is polarized along x and illuminates the bottom metal surface at normal incidence. (b) Top view.

#4821 - $15.00 US Received 16 July 2004; revised 23 September 2004; accepted 2 October 2004

The electric and magnetic field strengths of the input pulse in the substrate, linearly polarized along x, are given by $E_{x,\,in}(z,t) = A_{in}\cos\left[\omega_{in}t - (2\pi n_s/\lambda_{in})z\right]$ and $H_{y,in}(z,t) = n_s\sqrt{\varepsilon_0/\mu_0}E_{x,in}(z,t)$. Here, A_{in} is taken as a *Gaussian* shaped function $A_{in} = A_0\exp\left[-2\ln(2)\left\{(t-t_0-n_s z/c)/\tau_0\right\}^2\right]$, where A_0 is the field amplitude. The parameters t_0 and τ_0 are an arbitrarily chosen delay time and the pulse width, respectively.

The spatio-temporal evolution of the field distribution in the air-filled channel connecting the top and bottom holes is accompanied by a Poynting flow $S_z = \left(\vec{E}\times\vec{H}\right)_z$ (W/cm^2) along the *z*-axis. We define $s_z = \frac{1}{F}\int S_z(x,y)dxdy$ as the mean value of S_z inside one hole, where the integral is taken over the hole cross section of area *F*. The time average of s_z, taken over one cycle $T = 2\pi/\omega_{in}$, is indicated as $\bar{s}_z$. Finally, a normalized quantity is introduced, $\bar{s}_{z,norm} = \bar{s}_z/\bar{s}_{in,\max}$ where $\bar{s}_{in,\max} = n_s c\varepsilon_0 A_0^2/2$ denotes the power density at the peak of the input signal. In addition, the energy density W_e is of interest. For instance, $W_{ex} = \frac{1}{2}\varepsilon_0 E_x^2$ describes the instantaneous energy density of E_x in air. We define again a mean value w_{ex}, a time average $\bar{w}_{ex}$ and an energy density $\bar{w}_{ex,norm}$, normalized to $\bar{w}_{in,\max} = n_s^2\varepsilon_0 A_0^2/4$.

The time-dependent near fields in the metal film are numerically calculated by applying a three-dimensional (3D) finite-difference time-domain code (FDTD) to Eqs. (1a-c), see, e.g., Ref. [29]. The incorporation of Eq. (1c) into Yee's FDTD scheme follows instructions given in Ref. [30], in connection with Eq. (4) therein. The space grid is composed of 200 (x direction) x 200 (y) x 210 (z) cells with space increments of 2.5nm in each direction. Periodic boundary conditions are applied to the sides of this unit cell in the x and y directions whereas perfectly matched layers (PML) terminate the FDTD lattice below and above the metal film. A computing time of almost 10 hours is needed to calculate the time evolution of the fields in a time interval of about 200 fs using a PC with an Intel Pentium 4 processor (2GHz).

Depending on n_s, different types of SPP modes will be excited at the metal/substrate interface. SPPs are characterized by their integer mode indices $(p,q)_i$, with $i = A$ for the air and $i = S$ for the substrate interface. *p* and *q* define the components of the plasmon wave vector $\vec{k}_{sp} = k_{sp,x}\vec{e}_x + k_{sp,y}\vec{e}_y$ in the x-y plane, i.e., $k_{sp,x} = \pm 2\pi\, p/a_0$ and $k_{sp,y} = \pm 2\pi\, q/a_0$ [13]. The dispersion relation for a SPP mode $(p,q)_i$ can be written as [7,13]

$$\omega(p,q)_i = \frac{2\pi c\sqrt{p^2+q^2}}{a_0 n_i}\sqrt{\frac{\varepsilon_m + n_i^2}{\varepsilon_m}} \tag{3}$$

Equation (3) is derived from the SPP dispersion relation for a *smooth* metal film (interface) without holes. It is believed to be a good approximation even for perforated metal films as long as the hole diameter is much smaller than a_0 [2]. The corresponding vacuum wavelength of the exciting light is $\lambda(p,q)_i = 2\pi c/\omega(p,q)_i$.

In the following simulations, the carrier wavelength of the incident light pulse, $\lambda_{in} = 530$ nm, is much larger than the maximum cutoff wavelength $\lambda_c = \pi d/1.841 \approx 213$ nm for a cylindrical metallic channel of diameter $d = 125$ nm [31]. Thus, light transmission through the channel is possible only via photon tunneling supported by evanescent fields of exponentially decaying amplitude. Strictly speaking, this describes only the situation inside a

#4821 - $15.00 US Received 16 July 2004; revised 23 September 2004; accepted 2 October 2004

channel of a perfect metal, where the propagation constant is purely imaginary. For a real metal, however, also damped propagating modes with non-vanishing real part of the propagation constants exist [12, 15]. This explains the appearance of a damped real power flow, i.e., a non-vanishing time-averaged Poynting vector along the channel axis, as well as enhanced light tunneling through the channel in the case of finite conductivity.

3. Calculated power flow and energy density inside a hole channel

In this section, we first analyze the temporal dynamics of the photon flux inside the nanoholes. Figure 2 shows the time evolution of the mean photon flux density $\bar{s}_{z,norm}$ inside a hole channel at the bottom (black lines) and top (red lines) surfaces for various values of the refractive index n_s of the substrate. The photon flux is directed upward, from bottom to top, if $\bar{s}_{z,norm} > 0$ and downward if $\bar{s}_{z,norm} < 0$. The incident 10 fs pulse is indicated in Fig. 2(a).

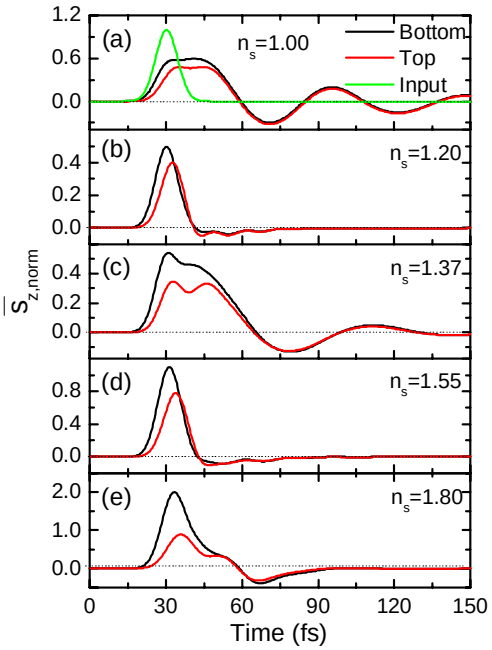

Fig. 2. *Photon flux* density $\bar{s}_{z,norm}$ vs time in a hole channel at z = 0, (bottom interface, black) and z = h (top interface, red) for substrate refractive indices n_s = 1.00 to 1.80, (a)-(e).The input pulse (green) is shown in (a).

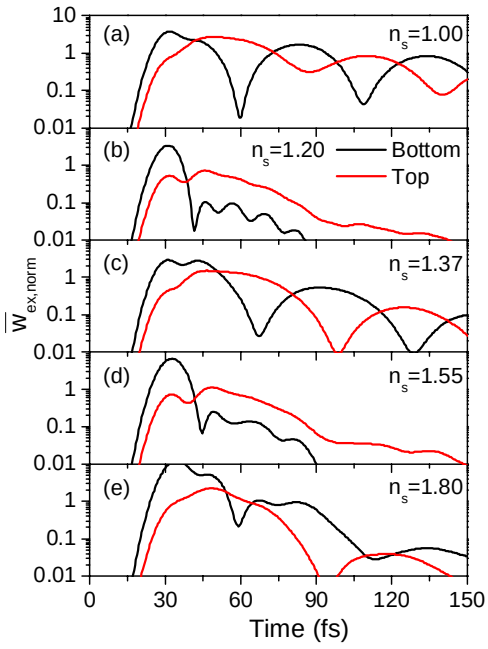

Fig. 3 *Field energy* density $\bar{w}_{ex,norm}$ vs time inside a hole at z = 0 (black line) and at z = h (red line) for n_s = 1.00 to 1.80, (a)-(e).

In Fig. 3 we compare these results to the time evolution of the mean electric field energy density $\bar{w}_{ex,norm}$ inside a hole at the bottom ($z = 0$) and top ($z = h$) interface. One sees that the curves in Figs. 2(a), (c) and (e) on one hand and those of Figs. 2(b) and (d) on the other hand are significantly different. Figures 2(b) and (d) indicate a noticeable photon flux only as long as the incident pulse is present. The curves in Figs. 2(a), (c) and (e) show quite pronounced, rather long lived oscillations persisting after the incident pulse vanished (t > 40fs). Similar oscillations are also seen in Figs. 3(a), (c) and (e). These oscillations occur when the excitation laser is resonant with SPP excitations at **both** the bottom and top interfaces and directly reflect the coherent coupling between SPP excitations at both interfaces. Using Eq. (3) one finds SPP resonances $(p,q)_S$ at the substrate interface at $\lambda(\pm 1,0)_S = 521$ nm at $n_s = 1.0$, $\lambda(\pm 1,\pm 1)_S = 525$ nm at $n_s = 1.37$ and $\lambda(\pm 2,0)_S = 523$ nm

#4821 - $15.00 US
Received 16 July 2004; revised 23 September 2004; accepted 2 October 2004

at $n_s = 1.80$. For $n_s = 1.20$ and $n_s = 1.55$, however, all resonances are detuned by more than 50 nm from the air/metal SPP resonance $\lambda(\pm 1, 0)_A = 521$ nm.

In all cases, a considerable fraction of the incident pulse is directly coupled into the nanoholes, tunnels through the holes and is emitted into the far-field on the other side of the metal film (first peak in Figs. 3(a-e)). Another fraction is coupled into SPP radiation at the metal/air interface. This fraction may either be reemitted into the far field by scattering off the nanoholes or be absorbed by the metal due to Ohmic losses.

Previous results from a 1-D slit model indicate a strong initial response to an incident 10 - 50 fs light pulse followed by intensity oscillations persisting, surprisingly, for more than 100fs [20]. A quantitative comparison of our results to those of Ref. [20] is difficult, in particular, since the transmission spectra in [20] seem to depend on the incident pulse duration which is not expected for linear optical spectra. Our results are in quite good qualitative agreement with experiments on THz pulse transmission through two-dimensional aperture arrays in metals [25]. There a non-resonant transmission related to the simple transmission through the apertures was found being followed by a resonant transmission (periodic oscillations) related to the interaction of the THz pulse with SPP excitations. A more quantitative comparison requires to consider the different geometries and dielectric functions which is beyond the scope of this work.

In the case of nonresonant SPP excitation ($n_s = 1.20$ and 1.55), the approximately exponential decay of the second peak in Fig. 3(b,d) directly reflects the lifetime of these SPP excitations of about 20 fs. This short lifetime is mainly determined by radiative scattering losses at the holes [6]. The presence of these two distinct transmission channels, direct tunneling through the holes vs. SPP re-radiation gives rise to a non-exponential decay of the energy density at the metal/air interface.

In the case of resonant SPP excitation ($n_s = 1.0$, 1.37 and 1.80), the incident pulse, in addition to being directly coupled into the nanohole channel, can now also excite SPPs at the bottom interface. Thus, coherent coupling between SPP modes at both interfaces, mediated by photon tunneling through the holes, may now influence the transmission dynamics. This coupling can well be described in a classical coupled mode model. The coupling induces an energy transfer between both modes with a yield $\rho = |V/\Omega|^2$ and a beating period $T = \pi/\Omega$ with $\Omega = \sqrt{\Delta\omega^2/4 + |V|^2}$, where, $\Delta\omega = \omega(1,0)_A - \omega(p,q)_S$ is the detuning between the two coupled SPP modes and $|V|$ is the coupling strength.

For $n_s = 1.0$ the coherent coupling effects are most pronounced and give rise to the periodic energy transfer between top and bottom interface (Fig. 3(a)). In this case, the SPP eigenmodes at both interfaces are degenerate and the beating period $T = \pi/|V|$ is a direct measure of the coupling strength. The beating period of $T \approx 50$ fs corresponds to a coupling strength of about 40 meV. Here, $\rho = 1$, i.e., the energy transfer between both modes is complete, in quite good agreement with the simulated results. The overall damping of the energy density occurs on a 50 fs time scale, much slower than in the off-resonant case. This suggests that the newly formed coupled SPP mode is less efficiently scattered into the far-field than the uncoupled $(1,0)_A$ mode. This quite surprising result needs further theoretical investigations of the interplay between the spatial SPP mode profile and radiative damping.

For $n_s = 1.37$, the SPP resonances at the two interfaces, $(1,0)_A$ and $(1,1)_S$ are no longer identical but their detuning is rather small, $\Delta\omega =$ 18 meV. The beat period seen in Fig. 3(c) is $T \approx$ 60 fs and one obtains $|V| \approx$ 34 meV and $\rho \approx$ 0.94. Thus, both $|V|$ and ρ are only slightly different from the values for $n_s = 1.0$. A marked difference between Figs. 3(a) and (c) is the faster decay of the energy density for $n_s = 1.37$ (about 30 fs), indicating a stronger

#4821 - $15.00 US Received 16 July 2004; revised 23 September 2004; accepted 2 October 2004

radiative damping of the coupled SPP mode for $n_s = 1.37$. The values deduced for the coupling strength, detuning and transfer probability are similar for the case of $n_s = 1.80$. The most pronounced difference between the transmission dynamics in Figs. 3(c) and 3(e) is the stronger radiative damping for $n_s = 1.80$, now occuring on a time scale of about 22 fs.

The more rapid damping with increasing n_s is likely to reflect the increase in SPP scattering rate at the bottom interface which results from the smaller effective wavelength within the dielectric. The observed trend is at least in qualitative agreement with the Rayleigh scattering model for SPP damping [6].

In both nonresonant cases the detuning $\Delta\omega$ is large (more than 100 meV) and thus $\Delta\omega/2 > |V|$. Then T and ρ reduce to $T \approx 2\pi/\Delta\omega$ and $\rho \approx |2V/\Delta\omega|^2$. One gets $T \approx$ 9.5 fs for $n_s = 1.2$ and $T \approx$ 12 fs for $n_s = 1.55$. These times agree quite well with the modulation periods (11 fs and 15 fs) of the ripples on the curves of the energy density at the bottom interface (Fig. 3(b,d)). This reflects an inefficient energy exchange, $\rho \ll 1$.

In Ref [21] we have calculated the photon flux through hole arrays of different hole diameters d in a free-standing metal film. It was found that the beating period T decreases with increasing d. This means that the coupling strength V increases with d. On the other hand, one expects that V decreases with increasing thickness h of the metal film, since in a two-dimensional hole array the coupling between the fields on the two surfaces is essentially due to photon tunneling and thus the coupling decreases with increasing h, see also [14]. This is different for 1-D or slit gratings [12] where at least one propagating mode exists and thus pronounced Fabry-Perot effects may lead to a nonmonotonous variation of the coupling constant.

These results indicate that a classical coupled mode model reproduces many of the trends observed in our simulations. The important parameter in this description is the coupling strength V. It is generally proportional to overlap integrals of type $I = \left| \iint \vec{E}_{sp,S}(x,y)\, \vec{E}^{*}_{sp,A}(x,y)\, dxdy \right|$, where $\vec{E}_{sp,S}$ and $\vec{E}_{sp,A}$ denote the SPP eigenmodes at the lower and upper interfaces, respectively. Assuming that the integration extends over one unit cell [16], one sees that I has a maximum value in the degenerate case, $\vec{E}_{sp,S} = \vec{E}_{sp,A}$, corresponding to $(1,0)$ excitation at both interfaces. For excitation of $(1,1)_S$ or $(2,0)_S$ modes at the lower interface, however, the overlap integral is equal to zero, in contrast to the results of the full simulation. Much better agreement is achieved by assuming that integration extends only over the nanohole area *F*. We show in Section 4, that for all SPP eigenmodes (p,q), the spatial mode profile inside the nanoholes is rather well described by the diffraction pattern of a single aperture [32,33] and rather independent of the actual values of p and q. Thus similar magnitudes of the coupling strength are expected for the cases considered in Fig. 3 (a,c,e), in agreement with the actual simulations. This indicates that it is indeed appropriate to take integrations over the hole area to estimate the coupling. Similar overlap integrals may also be used to quantitatively describe the radiative damping of SPP modes.

Finally we emphasize that while such a simplified coupled mode picture is well suited for understanding the SPP coupling dynamics, it cannot reproduce the complex, asymmetric line shapes of the observed far-field transmission spectra. In the spectral domain, the non-exponential decay due to the interference between direct nonresonant transmission due to photon tunneling and resonant SPP reradiation translates into a complex, asymmetric Fano-like lineshape, as recently suggested theoretically [34] and confirmed experimentally [35]. The spectral lineshape of far-field transmission spectra resulting from our simulations will be addressed in detail elsewhere.

#4821 - $15.00 US Received 16 July 2004; revised 23 September 2004; accepted 2 October 2004

4. Spatial near-field SPP mode profiles

The time-dependent pulse transmission results presented in Section 3 indicate that the transmission dynamics and thus the linear optical spectra of these nanostructures depend critically on the spatial near-field profiles of the excited SPP modes. Here, it is important that both the spatial and polarization properties in the optical near-field of the metal nanohole array are much different from that of the incident and transmitted far-field beam. Experimentally, one finds that as long as the wavelength of the incident pulse is larger than the grating constant a_0, the polarization, propagation direction and beam divergence of the transmitted beam is almost identical to that of the incident beam, as only the zeroth diffraction order of the grating is transmitted. Yet, the diffraction of the incident beam at the subwavelength holes gives rise to polarization conversion and rather complicated mode profiles in the optical near-field which so far have been studied experimentally [22] and theoretically [13,21] only to a limited extent. Here, we discuss the mode profiles for two specific values of the substrate refractive index, $n_s = 1.37$ and 1.80, corresponding to excitation of $(1,1)_S$ and $(2,0)_S$ SPP modes at the metal/dielectric interface, respectively.

4.1 $n_s = 1.37$

Figures 4 and 5 show spatial field distributions for a substrate refractive index of $n_s = 1.37$. The data are taken at a fixed instant in time, $t = 45$ fs, i.e., 15 fs after the maximum of the 10 fs incident pulse, a time when the incident pulse has already vanished but still some energy is stored in SPP excitations. The top images show the distribution within a unit cell around one hole in the x-y plane in air at $z = h + 2.5$ nm, i.e., 2.5 nm above the metal/air interface. The plots at the bottom apply to a plane in the substrate, $z = -2.5$ nm, 2.5 nm below the lower metal surface. Different polarization components of the *longitudinal* electric fields are shown in Fig. 4, namely (a) $\overline{E_x^2}$, (b) $\overline{E_y^2}$ and (c) $\overline{E_x^2} + \overline{E_y^2}$. Figure 5 shows the squared field strength of the *transversal* field, $\overline{E_z^2}$, polarized perpendicular to the interfaces.

An important result of these simulations is that the near-field distribution on both interfaces can be separated, to a fairly good approximation, into two distinct contributions: (i) the near-field inside a nanohole aperture and in its immediate vicinity, (ii) the SPP field on the flat metal surface. This is different from previous theoretical predictions [13].

The spatial distribution and polarization dependence closely above (top surface) and below (bottom surface) a nanohole agrees well with the results from the analytic Bethe-Bouwkamp model which describes the diffraction of a linearly polarized optical field by a small hole in a thin, perfectly conducting metal film [32,33]. Specifically, it predicts the excitation of rather strong E_y and E_z polarized fields, and the sharp peaks at the rim of the aperture. Outside the aperture, the model predicts $\overline{E_y^2} = \overline{E_x^2} = 0$ because of the perfect conductor assumption. The finite conductivity of a real metal modifies the Bethe-Bouwkamp solution by spatially smoothing the divergencies at the rim and allows for non-vanishing longitudinal fields on the metal surface in the vicinity of the aperture.

Also, for real metals, evanescent SPP modes can be excited which can then propagate along the metal surface. The SPP field on the flat metal surface reflects the interference pattern of the different SPP modes excited by the diffraction of light at the nanohole grating. Fig. 4(a) (top), e.g., shows a stripe pattern of $\overline{E_x^2}$ with a modulation period of $a_0/2$, with peak intensities at $x = \pm a_0/2$ and $x = 0$, perpendicular to the incident polarization direction. Equation (3) predicts resonant excitation of $(\pm 1, 0)_A$ SPP at the metal/air interface. Accordingly, these patterns are due to the interference of counter-propagating SPP-fields

#4821 - $15.00 US Received 16 July 2004; revised 23 September 2004; accepted 2 October 2004

running along the x-direction with wave vectors $k_{sp,x} = \pm 2\pi / a_0$ and $k_{sp,y} = 0$, in good agreement with the experimental findings [22]. Higher order SPP modes with $k_{sp,x} = \pm m 2\pi / a_0, m > 1$ are much less efficiently excited.

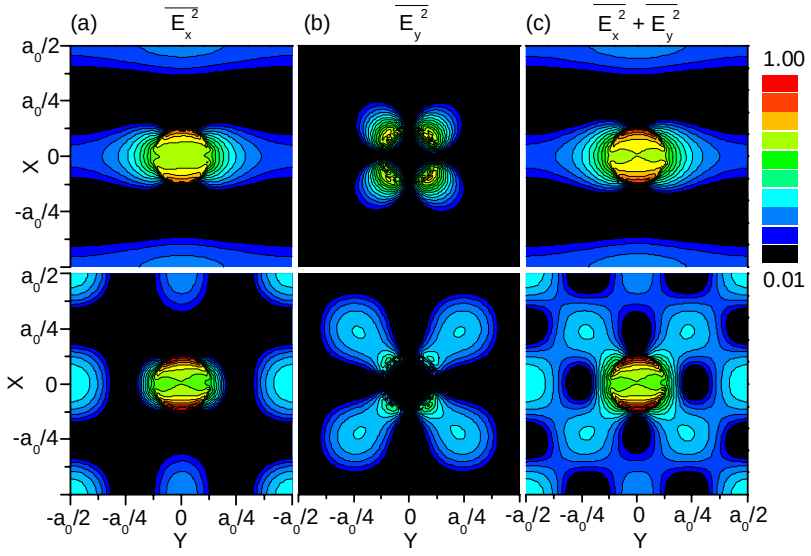

Fig. 4. Spatial distribution of time-averaged squared electric field strengths (a) $\overline{E_x^2}$, (b) $\overline{E_y^2}$, (c) $\overline{E_x^2} + \overline{E_y^2}$ in the x-y planes of the substrate/metal interface (bottom row, $z = -2.5$ nm) and the air/silver interface (top row, $z = h + 2.5$ nm) at time t = 45fs. The refractive index of the substrate is $n_s = 1.37$ and the incident beam is polarized along the x-direction. A logarithmic color scale is used. The intensity of $\overline{E_y^2}$ at the top interface (b) is enhanced by a factor of 10.

The SPP mode at the bottom, substrate/metal interface, shows a more complicated wave pattern with a period of $a_0 / 2$ along both the x- and y-direction [Fig. 4 (bottom)]. The essential features are described by interference of $(\pm 1, \pm 1)_S$ SPP waves. To show this in a simple way we consider two monochromatic SPP fields, $\vec{E}_+$ and $\vec{E}_-$, with $\vec{E}_\pm = \{\cos[\omega t + k(x \pm y)] + \cos[\omega t - k(x \pm y)]\}(\vec{e}_x \pm \vec{e}_y)$ and $k = |k_{sp,x}| = |k_{sp,y}|$ The field $\vec{E}_+$ is composed of an $(+1,+1)$ wave ($k_{sp,x} = k_{sp,y} = +2\pi / a_0$) and a counter-propagating $(-1,-1)$ wave whereas $\vec{E}_-$ is a superposition of $(+1,-1)$ and $(-1,+1)$ waves. From $\vec{E}_+$ and $\vec{E}_-$ we get time-averaged squared field strengths $\overline{E_x^2} \propto \cos^2(kx)\cos^2(ky)$ and $\overline{E_y^2} \propto \sin^2(kx)\sin^2(ky)$, which are similar to the wave pattern in Fig. 4 (bottom row). This excitation of the $(\pm 1, \pm 1)_S$ modes is expected from the simplified dispersion relation, Eq. (3).

#4821 - $15.00 US
Received 16 July 2004; revised 23 September 2004; accepted 2 October 2004

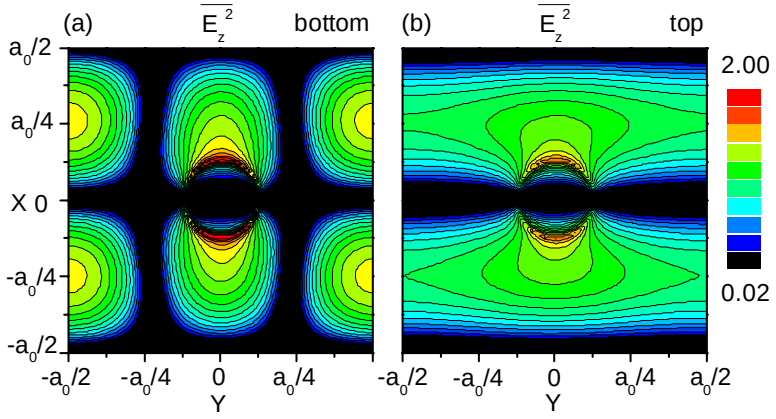

Fig. 5. Same as Fig. 4 but squared z-component of the electric field, $\overline{E_z^2}$ at the substrate/silver interface at $z = -2.5$ nm (a) and at the air/silver interface at $z = h + 2.5$ nm (b). A logarithmic color scale is used.

The spatial distribution of the transversal z-component of the electric fields $\overline{E_z^2}$ at the air/metal interface, Fig. 5(b), shows a standing wave with a period of $a_0/2$ and maxima at $x = \pm a_0/4$, phase shifted by $\Delta x = a_0/4$ with respect to $\overline{E_x^2}$. The same phase shift $\Delta x = a_0/4$ is also seen when comparing $\overline{E_z^2}$ and $\overline{E_x^2}$ at the substrate/silver interface (Figs. 5(a) and 4(a)). These phase shifts result directly from Maxwells's laws for evanescent SPP waves.

It is important to note that the appearance of polarization mixing and the excitation of $(\pm 1, \pm 1)$ SPP modes in the present case of input polarization along the x-axis is caused by the diffraction of the incident light at subwavelength holes and only occurs in the optical near-field of the film. The transmitted far-field is polarized along the incident polarization direction and is a plane wave propagating along the z-direction. The results show that the metal nanohole array basically serves as an efficient spatial SPP mode filter, selecting primarily $(\pm 1, 0)_A$ SPP modes at the top and $(\pm 1, \pm 1)_S$ SPP modes at the bottom interface, as predicted by the dispersion relation for a planar metal film.

Finally, we point to the fact that the separation of the near-field into a Bethe-Bouwkamp solution inside and in the immediate vicinity of the holes and planar metal film SPP modes outside the holes is of course only an oversimplification and some perturbations occur in the vicinity of the holes due to the coupling between both fields. For excitation of low order $(1,0)$ and $(1,1)$ SPP modes these perturbations are relatively small.

4.2. $n_s = 1.80$

Figure 6 shows the spatial distributions of (a) $\overline{E_x^2}$ and (b) $\overline{E_z^2}$ on the air/metal interface (top) and the substrate/metal interface (bottom) for a substrate of refractive index $n_s = 1.80$. The field distribution at the top interface is very similar to that for $n_s = 1.37$, i.e., only weakly affected by the coupling between SPP at the top and bottom interfaces. The spatial distribution at the substrate/metal interface near the nanoholes is again well described by the Bethe-Bouwkamp solution. The SPP intensity pattern outside the holes now shows a modulation period of $a_0/4$, i.e., results from interference of counterpropagating SPP waves with wave

#4821 - $15.00 US
Received 16 July 2004; revised 23 September 2004; accepted 2 October 2004

vector $k_{sp,x} = \pm 4\pi / a_0$. This excitation of $(\pm 2, 0)_S$ modes directly follows from Eq. (3). The spatial shift between the mode patterns of $\overline{E_x^2}$ and $\overline{E_z^2}$ by $a_0/8$ can be understood again by applying Maxwells' laws to the evanescent SPP fields.

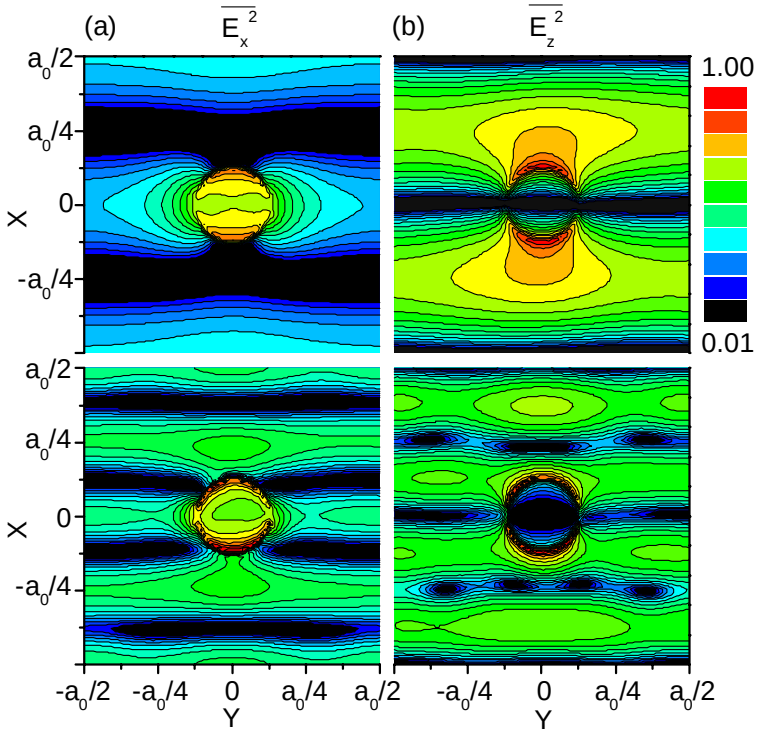

Fig. 6. Time-averaged squared field strength on the substrate/silver interface (bottom row) and the air/silver interface (top row) at time t = 45fs (logarithmic color scale). (a) $\overline{E_x^2}$, (b) $\overline{E_z^2}$. The refractive index of the substrate is $n_s =$ 1.80. The intensity scale for $\overline{E_z^2}$ at the bottom interface is from 0.01 to 10.

Looking at these results in some more detail, one finds that the simplified interpretation in terms of diffraction by a single aperture and SPP modes of a planar metal film holds not quite as well as in the case of $n_s = 1.37$. The coupling between these two contributions explains the differences.

5. Spatio-temporal evolution of the SPP fields

In the following we present movie sequences of the temporal development of the spatial SPP near-field distribution after impulsive excitation for three different values of the substrate refractive index, $n_s = 1.00$ (Fig. 7), $n_s = 1.37$ (Fig. 8), and $n_s = 1.80$ (Fig. 9). These figures show the sum of the squared field strengths of the longitudinal field components $\overline{E_x^2}(x, y, z, t) + \overline{E_y^2}(x, y, z, t)$ in an x-y plane slightly below the lower interface, $z \equiv -2.5nm$ (left plot) and slightly above the upper interface, $z \equiv h + 2.5nm$ (right plot). We note that the contribution of the y-component $\overline{E_y^2}(x, y, z, t)$ is significant only for $n_s = 1.37$ and is negligibly small in the other two cases. The squared fields are averaged over one optical cycle. The movie sequences comprise a time interval between 15 fs and about 200 fs. The peak intensity of the incident 10fs pulse arrives at the bottom interface at t = 30 fs. Four hole

#4821 - $15.00 US
Received 16 July 2004; revised 23 September 2004; accepted 2 October 2004

apertures with centers at $x = +0.25$ μm, $y = \pm 0.25$ μm and $x = -0.25$ μm, $y = \pm 0.25$ μm are included in each plot.

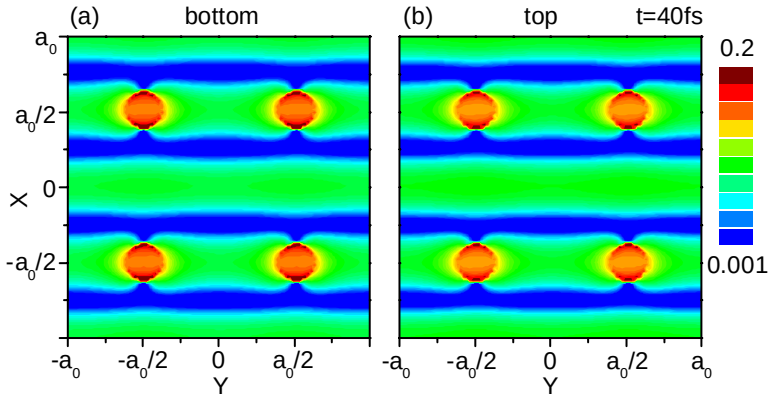

Fig. 7. Movie sequences showing the time evolution of squared electric field strengths, averaged over one optical period $T = 2\pi/\omega$, in the x-y-plane (logarithmic color scale) at (a) the bottom (t = 40fs) and (b) the top interface (t = 40 fs) for a freestanding metal film, n_s = 1.00, and excitation with a 10fs optical pulse (3.9 MB movie).

Figure 7 displays the dynamics of $\overline{E_x^2} + \overline{E_y^2}$ in the case of a free-standing metal, $n_s = 1.00$, where $(\pm 1,0)$ SPP Bloch modes are excited at both interfaces. One sees that the spatial field distribution does not vary significantly with time, apart from the interval between 20 and 40 fs, when the incident pulse is still present at the bottom interface. During its presence, the field intensity at the hole centers is much stronger than at later times. This reflects the transmission dynamics due to photon tunneling. Due to this direct tunneling, a considerable fraction of the field intensity appears with a delay of only 1 to 2 fs at the metal/air interface. The intensity profile of this initial transmission peak basically follows the time profile of the incident pulse (see also Fig. 3(a)). This indicates that time delays associated with the transit time of photons through the nanohole channel are negligible. After this initial pulse has vanished, see e.g. the images at t=40 fs, the mode patterns are governed by SPP interference. In our simulations we find at least five periods of coherent energy exchange between the bottom and top interfaces, reflecting a SPP lifetime that is much longer than the 10 fs pulse duration.

Finite time delays have recently been observed in ultrafast pulse transmission experiments [24,6]. Our results indicate that such delays reflect the finite lifetime of the SPP excitation and not the photon tunneling of only 1 to 2 fs. Such delays will be seen in transmission experiments performed with pulses that are longer in duration than the SPP lifetime, whereas the full and complex SPP time dynamics will only be revealed if much shorter pulses with durations in the 10 fs range are used. In the case of a freestanding metal film with sufficiently small hole diameters and thus long SPP lifetimes [6], this dynamics is largely dominated by the periodic and almost complete energy transfer between SPP modes at bottom and top interfaces, as seen from the time evolution of the SPP field at times larger than 40 fs.

#4821 - $15.00 US Received 16 July 2004; revised 23 September 2004; accepted 2 October 2004

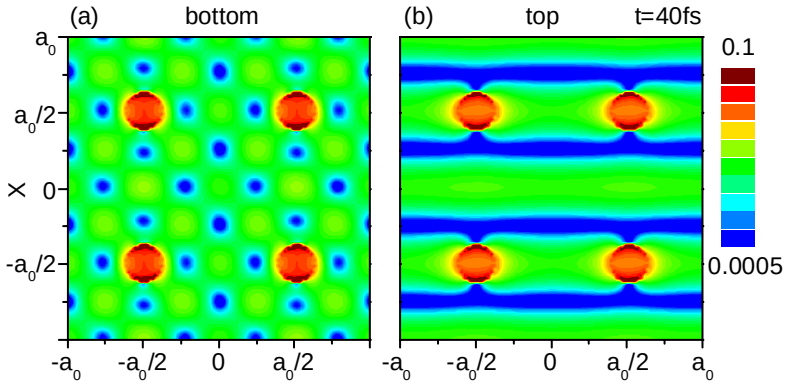

Fig. 8. Movie sequences showing the time evolution of squared electric field strengths in the ***x***-***y***-plane (logarithmic color scale) at (a) the bottom (t = 40 fs) and (b) the top interface (t = 40 fs) for n_s = 1.37, and excitation with a 10fs optical pulse (3.4 MB movie).

The spatio-temporal evolution of $\overline{E_x^2} + \overline{E_y^2}$ for $n_s = 1.37$ (Fig. 8) at the top air/metal interface is similar to that seen in Fig. 7 and reflects again the initial nonresonant tunneling contribution at early times and the coherent coupling and energy exchange between SPP modes at both interfaces at later times. Now the damping time of the SPP fields is much shorter than for the freestanding films and amounts to about 30 fs instead of 50 fs for $n_s = 1.0$.

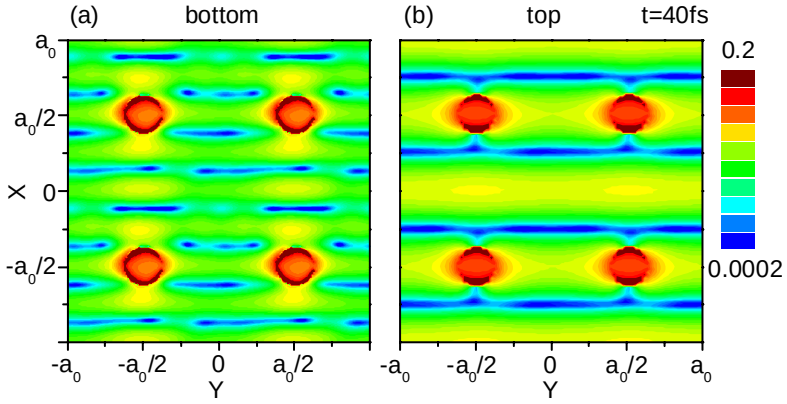

Fig. 9. Movie sequences showing the time evolution of squared electric field strengths in the *x*-*y*-plane (logarithmic color scale) at (a) the bottom and (b) the top interface for n_s = 1.80, and excitation with a 10fs optical pulse (2.8 MB movie).

The field distributions at the bottom interface now reflects the interfering $(\pm 1, \pm 1)$ SPP modes. The initial SPP field dynamics during the presence of the inicident pulse is rather complex and shows the rapidly changing interference pattern between incident laser pulse and resonant SPP excitations.

The field dynamics for $n_s = 1.80$ (Fig. 9) is in general rather similar to that for $n_s = 1.37$, apart from the fact that now $(\pm 2, 0)$ SPP modes are excited at the lower interface. The faster SPP damping time now limits the number of clearly visible energy transfer cycles between bottom and top interface to 2.

#4821 - $15.00 US
Received 16 July 2004; revised 23 September 2004; accepted 2 October 2004

6. Summary and conclusions

In summary, we have presented a three-dimensional time and space resolved simulation of ultrafast light propagation through a silver film perforated with a periodic array of nanoholes. We have studied the propagation of 10 fs optical pulses shorter in duration than the damping time of SPP excitations. The wavelength of the input pulses was chosen such as to excite $(\pm 1,0)$ SPP Bloch modes at the top air/silver interface and the refractive index of the substrate was varied in order to study coherent coupling dynamics of SPP excitations at both interfaces of the metal film.

Several important conclusions can be drawn. First, spatial near-field profiles give direct evidence for the resonant excitation of surface plasmon polaritons at the surfaces of the metal film and support models that describe the optical properties of these nanostructures as those of a plasmonic crystal. Two distinct transmission channels exist. First, a fraction of the incident light directly tunnels through the hole channel and is rescattered into the far-field on the other side of the film. The transit time of this nonresonant tunneling contribution is negligibly small. Second, SPP can be excited at either interface by the grating coupler effect at certain resonance energies. SPP modes at the top and bottom interfaces are coupled via photon tunneling through the nanohole channel and eventually rescattered into far-field radiation. The simulations indicate that for small hole diameters, i.e., sufficiently long radiative SPP lifetimes, a strong coupling regime can be achieved between SPP Bloch modes of different order at the two interfaces if these modes are energetically tuned into resonance by variation of the substrate refractive index. Models based on coupled mode theory account for this behavior. The linear optical far-field transmission spectra result from the interference between these two transmission channels mentioned above. Our results not only shed light on the complex SPP dynamics in these quasi-two-dimensional plasmonic crystals but also suggest different strategies for tailoring their optical properties. Specifically, the quality factor of the SPP transmission resonances can be enlarged by tailoring the radiative SPP damping time and transmission enhancement can be improved by optimizing the coupling between SPP modes at both interfaces. This makes plasmonic nano-crystals interesting building blocks for future nano-photonic devices with applications, e.g, in nano-photolithography or ultrafast microscopy.

Acknowledgments

We thank A. Knorr , J. Förstner, Q. H. Park and D. S. Kim for helpful discussions and V. Malyarchuk for help during the early stage of this work. Financial support by the Deutsche Forschungsgemeinschaft (SFB 296) and the European Union (SQID) is gratefully acknowledged.

#4821 - $15.00 US Received 16 July 2004; revised 23 September 2004; accepted 2 October 2004